Materials Research Bulletin 55 (2014) 19–25

Contents lists available at ScienceDirect

Materials Research Bulletin

journal homepage: www.elsevier.com/locate/matresbu

Modification of Bi:YIG film properties by substrate surface ion pre-treatment

A.N. Shaposhnikov [a], A.R. Prokopov [a], A.V. Karavainikov [a], V.N. Berzhansky [a], T.V. Mikhailova [a], V.A. Kotov [b], D.E. Balabanov [c], I.V. Sharay [d], O.Y. Salyuk [d], M. Vasiliev [e], V.O. Golub [d,*]

[a] Taurida National V.I. Vernadsky University, Vernadsky Avenue, 4, Simferopol, 95007, Ukraine
[b] V.A. Kotelnikov Institute of Radio Engineering and Electronics, RAS, 11 Mohovaya Street, Moscow, 125009, Russia
[c] Moscow Institute of Physics and Technology, Dolgoprudny, 141700, Russia
[d] Institute of Magnetism, NAS of Ukraine, 03142, Kiev, Ukraine
[e] Electron Science Research Institute, Edith Cowan University, 270 Joondalup Drive, Joondalup 6027, Australia

ARTICLE INFO

Article history:
Received 28 July 2013
Received in revised form 13 December 2013
Accepted 31 March 2014
Available online 02 April 2014

Keywords:
A. Magnetic materials
A. Structural materials
B. Sputtering
D. Optical properties
D. Magnetic properties

ABSTRACT

The effect of a controlled ion beam pre-treatment of (111)-oriented $Gd_3Ga_5O_{12}$ substrates on the magneto-optical properties and surface morphology of the ultrathin bismuth-substituted yttrium–iron garnet films with a composition $Bi_{2.8}Y_{0.2}Fe_5O_{12}$ was studied. It has been shown that the observed sign inversion of magneto-optical effects (Faraday rotation and magnetic circular dichroism) observed in films that were deposited on the GGG substrate pre-treated by 1 keV and 4 keV Ar^+ ion beams is a result of the substrate surface amorphization caused by the ion bombardment.

© 2014 Elsevier Ltd. All rights reserved.

1. Introduction

Bismuth-substituted yttrium–iron garnet (Bi:YIG) films are often used as basic elements of one-dimensional magneto-photonic crystals (1D-MPC) as they exhibit high transmittance and large specific Faraday rotation (FR) in the visible and near-infrared optical spectrum regions [1–4]. Depending on the 1D-MPC optical spectrum operating range, the thicknesses of these films can vary from a few tens to several hundred nanometers. The structural quality of the magneto-active layer and in particular, characteristics of film-substrate transitional interface can significantly affect the 1D-MPC parameters such as the FR magnitude and transmittance. So the investigation of the optical and magneto-optical (MO) properties of ultra-thin Bi:YIG films, as a function of the substrate surface condition, are of great interest. The understanding of the kinetics of the film growth processes will further aid to the development of the new generation of MO devices.

Ferrites with garnet structures are ferrimagnetics with three magnetic sublattices: octahedral (*a*), tetrahedral (*d*) and dodecahedral (*c*) sublattices [5]. The magnetizations of *a* and *c* sublattices have the same direction and are opposite to magnetizations of *d* sublattice. The direction of the integral magnetization vector in pure bismuth ferrite garnet is determined by *d* sublattice. However, partial substitution of magnetic ions may lead to decrease of *d* sublattice magnetization, and the integral magnetization direction of such a garnet can be determined by *c* and *a* sublattices. The situation when the magnetizations of the sublattices compensate each other and the integral magnetization turns into zero is called a magnetic compensation point. For some garnets compositions, due to the different temperature dependences of the sublattices magnetization, the compensation point can be reached varying the temperature. The transition through the compensation point is accompanied by the FR sign change.

It should be noted that there is a lack of information in the literature about the relation between properties of ultrathin Bi:YIG films and the state of the substrate surface. The formation of a transitional non-magnetic layer on the film-substrate interface of the $Bi_2Dy_1Fe_4Ga_1O_{12}$ films deposited by rf-magnetron sputtering at room temperature was reported in [6]. Unfortunately, no information about the substrate surface pre-treatment was

* Corresponding author at: Institute of Magnetism, NASU and MESU, 36-B Vernadsky Street, 03142 Kiev, Ukraine. Tel.: +380 683608875; fax.: +380 444241020.
E-mail addresses: v_o_golub@yahoo.com, golub@imag.kiev.ua (V. Golub).

http://dx.doi.org/10.1016/j.materresbull.2014.03.035
0025-5408/© 2014 Elsevier Ltd. All rights reserved.

presented in this paper. An impeded epitaxial growth of $(GdBi)_3(Fe,Al,Ga)_5O_{12}$ garnet films sputtered and in situ crystallized on the (111)-oriented $(GdCa)_3(Ga,Mg,Zr)_5O_{12}$ and $Sm_3(Ga,Mg,Zr)_5O_{12}$ garnet substrates bombarded by low-energy (100 eV) Ar^+ ions before the films deposition was discussed in [7]. Reflection high-energy electron diffraction data analysis showed that impeded growth is related to the bombardment-induced bond angles disorder on the substrate surfaces, mainly produced by the re-sputtering of oxygen. The reported thickness of the damaged layer was of about 0.5 nm. The formation of structurally damaged 12 nm thick layer on the surface of epitaxial YIG films after the bombardment by 0.5–2 keV oxygen ions was also demonstrated in [8].

In this paper, we study the effects of controlled ion beam pre-treatment and pre-annealing of the gadolinium gallium garnet $Gd_3Ga_5O_{12}$ (GGG) substrates on the MO properties (Faraday rotation and magnetic circular dichroism) of ultrathin Bi:YIG films.

2. Experimental

$Bi_{2.8}Y_{0.2}Fe_5O_{12}$ target was sintered using the conventional ceramics sintering technique. Bi:YIG films were deposited by reactive ion-beam sputtering technique on cold (111) GGG substrates in argon–oxygen mixture as described earlier [9–11]. The as-prepared films were amorphous. Film crystallization was performed in the air at normal atmospheric pressure at the temperature $T_{crys} = 650\,^{\circ}C$ during $t = 20$ min. The heating rate of the films at pre-crystallization annealing was ~40 °C/min. The films thickness, h, ranged from 2.9 nm to 180 nm. The thickness was calculated based on the sputtering rate (5.8 nm per minute) and the deposition times.

To determine the effect of substrate pre-treatment on the properties of synthesized Bi:YIG films, the substrates were processed before the film deposition by argon and oxygen ions with varying energy and current. The duration of ion pre-treatment was 5 min. Some of the GGG substrates were also pre-annealed in air at the atmospheric pressure. According to the substrates pre-treatment regimes, the films were divided into four types (see Table 1).

The specific Faraday rotation θ_F, the coercivity H_c, Curie T_C and compensation temperatures T_{comp} were determined from the Faraday rotation hysteresis loops (FRHLs) using the Faraday magneto-polarimeter operating at $\lambda = 655$ nm in 20–150 °C temperature range. The magnetic field was applied along the light beam direction and perpendicular to the film plane. Magnetic circular dichroism (MCD) spectral measurements were performed using a Jobin-Yvon dichrograph at $H = 5.5$ kOe in 270–850 nm wavelength range with the step 1 nm. The MCD signal was calculated as

$$\left[\frac{(I_+ - I_-)}{(I_+ - I_-)}\right]/h$$

where I_+ and I_- are the intensities of right- and left-hand circularly polarized light waves.

Table 1
The regimes of the substrate pre-treatment.

Film types	Gas	Ion energy	Ion current density ($mA\,cm^{-2}$)	Substrate pre-annealing
A	Argon	Low-energy plasma	1.0	–
B	Argon	Ion beam, 1.0 keV	2.5	–
C	Argon	Ion beam, 4.0 keV	5.0	–
D	Oxygen	Low-energy plasma	1.0	One hour at 800 °C (in air)

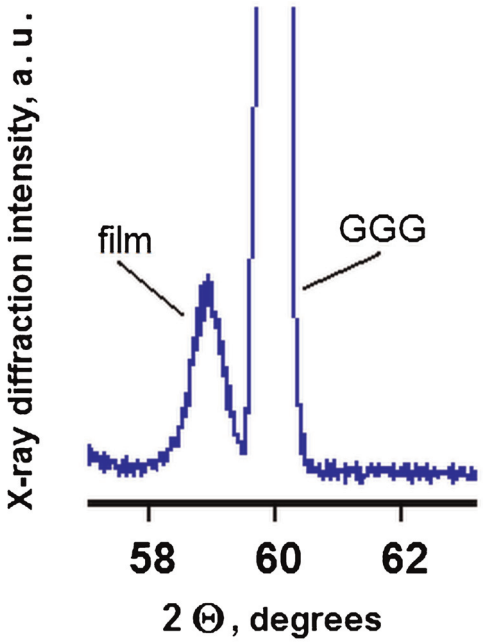

Fig. 1. XRD profile for 100 nm thick Bi:YIG A-type film. (For interpretation of the references to color in this figure legend, the reader is referred to the web version of this article.)

The structure of the samples was controlled by X-ray diffractometer. Solver PRO atomic force microscope (AFM) was used for the substrates and films surface visualization.

According to the electron probe microanalysis data, the composition of the thick Bi:YIG films was close to the target composition. This confirms the nearly equivalent composition transfer during the deposition. It also correlates with X-ray diffraction data showing a formation of the garnet epitaxial phase with a lattice parameter $a = 1.2602$ (see Fig. 1). The evaluation of Bi contents based on the Vegard's law [12] yields $X_{Bi} = 2.8$ atoms per formula unit (at./f.u.). The determined lattice mismatch between lattice parameters of the film and the substrate is $\Delta a = a_{film} - a_{sub} = 0.0208$ nm, $a_{sub} = 1.2383$ nm. The epitaxial growth of of Bi:YIG films has also been confirmed by our previous ferromagnetic resonance measurements [10].

3. Results and discussion

The dependences of the specific Faraday rotation θ_F on the films thicknesses, h, for three types of Bi:YIG films are shown in Fig. 2. The corresponding FRHLs are schematically shown in the insets. At

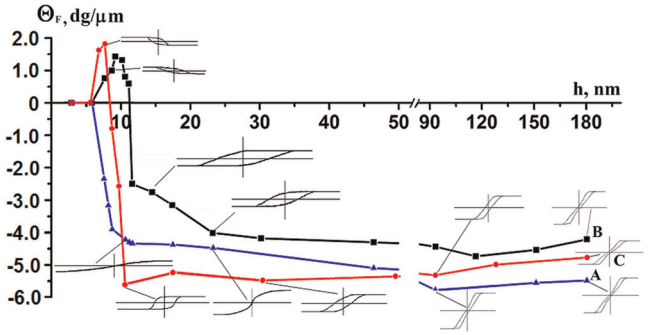

Fig. 2. θ_F (h) dependencies and Faraday hysteresis loops for the A-, B- and C-type films. (For interpretation of the references to color in this figure legend, the reader is referred to the web version of this article.)

room temperature, θ_F drops to zero for all film types when h is below 6 nm.

The A-type films demonstrate a negative θ_F and have an easy-plane or close to an easy-plane magnetic anisotropy for all thicknesses in the studied range, which is typical for the thick Bi:YIG films prepared using conventional techniques. However, the saturation magnetic field of the thin A-type films ($H_s \approx 4.5$ kOe) is much higher than that of the thick ones ($H_s \approx 1.0$ kOe). The Faraday rotation angle, θ_F, approaches the bulk material value for h, above 12 nm, which is approximately ten lattice periods. It reaches the lower limit, $\theta_F = -5.8°/\mu m$, for $h \geq 100$ nm. There is no compensation point in this type of films. The measured Curie temperature is $T_C \approx 350\,°C$.

A quite different behavior was observed for the B- and C-type films. Here, there is an interval of thicknesses where θ_F is positive. The Faraday rotation angle becomes negative only above a critical thickness, h_{cr} (10.6 nm for B-type films and 8.3 nm for C-type ones). The films display perpendicular anisotropy for all thicknesses in the $[h_{min}, h_{cr}]$ interval. The increase of Ar^+ ion energy as well as the ion beam current density leads to the narrowing of the interval, while the maximum value of θ_F becomes larger. Above h_{cr}, the Faraday rotation angle, θ_F, is negative. The observed FR sign inversion in the B- and C-type films is related to the variation of the compensation point temperature, T_{comp}, with the films thickness. Our measurements of T_{comp} for the B-type films show that it drops from 70 °C to 28 °C when h increases from 9.7 nm to 11.2 nm. Thus, for thin films with $h < h_{cr}$, the compensation point is above the room temperature, and the magnetization of their octahedral sublattices exceed the magnetization of the tetrahedral ones. Above the critical thickness, the situation is reversed. A similar change of T_{comp} with thickness is observed in the C-type films. Here, the compensation point drops below room temperature at a lower thickness (of about 8 nm).

The highest values of $\theta_F = -7.8°/\mu m$ at $\lambda = 655$ nm were obtained in 100 nm thick D-type films. The regimes of the substrate treatment for the D-type films were practically analogous to A-type films except for the fact that the oxygen plasma was used for the processing instead of argon plasma. As a result, the thickness dependence of FR for the D-type films is similar to the A-type one. The increase of the FR in these films is most probably related to lower destruction of the substrate surface at oxygen plasma treatment (decrease of breaking bond number on the surface and its amorphization).

The normalized MCD spectra for the B-type films of different thicknesses (8.7 nm, 11.6 nm, and 92.8 nm) measured at room temperature are presented in Fig. 3. The typical spectrum bismuth-substituted iron garnets [13–16] taken from [14] is also shown in Fig. 3 (curve 4) as a reference.

The reference spectrum and the spectra of the B-type films with $h > 10.6$ nm ($h > h_{cr}$; curves 2–3) exhibit a positively-valued peak at long wavelength and a negatively-valued peak at short wavelength, while for the thinner B-type films, the signs of the two peaks are reversed (curve 1, $h = 8.7$ nm $< h_{cr}$). In contrast, the MCD spectra for the A-type films do not change qualitatively with h and are similar to those of the B-type films with $h > 10.6$ nm. It is known [14,15] that the MCD spectra of iron garnets with bismuth content above 0.5 at./f.u. in the 295–730 nm wavelength range are mainly formed by the paramagnetic- and diamagnetic-type transitions with resonances at 299–318 nm, 394–432 nm and 477–521 nm. According to [15], the two transitions above 350 nm relate to the octahedral (a sublattice) [Fe^{3+}] and tetrahedral (d sublattice) [Fe^{3+}] sublattices and simultaneously involve iron-pair transitions. The intensity of the diamagnetic-type transitions for the iron garnets with low bismuth content and a high content of iron-substituting diamagnetic ions becomes comparable to the intensity of the main paramagnetic-type transition [16]. The decrease of the signal intensity, around 310 nm for thin B-type films, is due to the dilution of tetrahedral sublattice [15]. The MCD and the FR sign inversion at room temperature in the thin B- and C-type films is a result of the magnetization direction inversion of d and a sublattices with respect to the external magnetic field and the direction of electromagnetic wave propagation.

The thickness dependencies of the long-wave MCD peak position for A-and B-type films are shown in Fig. 4. For the A-type films with a thickness $5.8 < h < 10.6$ nm the position of the maximum of the long-wave MCD peak is located at 486 nm. For $h > 10.6$ nm it shifts to 490 nm. For B-type films when the thickness varies from 5.8 nm up to 23.2 nm the MCD peak position moves from 441 nm to 482 nm and then does not change with the thicknesses increase. So, the increase of the B-type film thicknesses leads to the shift of the MCD peak positions toward long-wave spectral area ("red shift").

It is known that the "red shift" depends on the Bi [17,18] and Fe [15,19] contents. The elements from substrate penetrate to the adjacent film layers leading to the decrease of Bi and Fe content. The increase of the film thickness is accompanied by the increase of these elements' mean concentrations. This can be clearly observed for the B-type films with thickness 5.8–23.2 nm. Subsequent growth of the film results in a return of the Bi and Fe mean concentrations to their nominal values. As it was mentioned above, the composition of the thick films practically coincides with the target composition. As for A-type films, a negligible value of "red shift" allows one to conclude that there is no appreciable variation

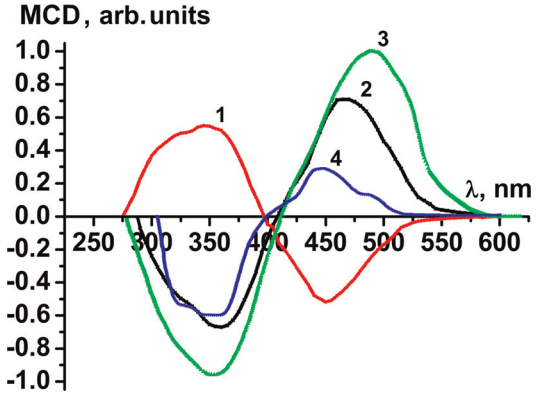

Fig. 3. Normalized MCD spectra for 8.7 nm (1), 11.6 nm (2) and 92.8 nm (3) thick B-type films and for 40 nm thick $Bi_{0.3}Pb_{0.1}Sm_{0.7}Gd_{0.2}Lu_{1.7}Fe_{4.3}Al_{0.5}Sc_{0.2}O_{12}$ film (4). (For interpretation of the references to color in this figure legend, the reader is referred to the web version of this article.)

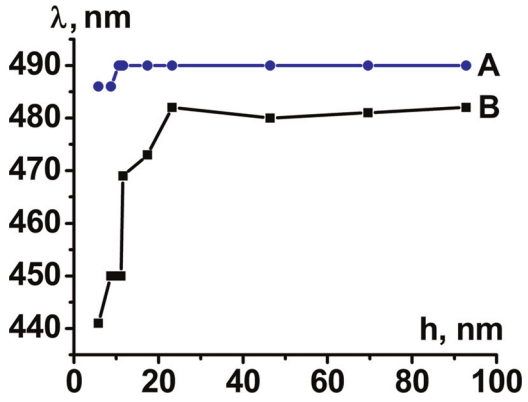

Fig. 4. Thickness dependence of the long-wave MCD peak position for the A- and B-type films. (For interpretation of the references to color in this figure legend, the reader is referred to the web version of this article.)

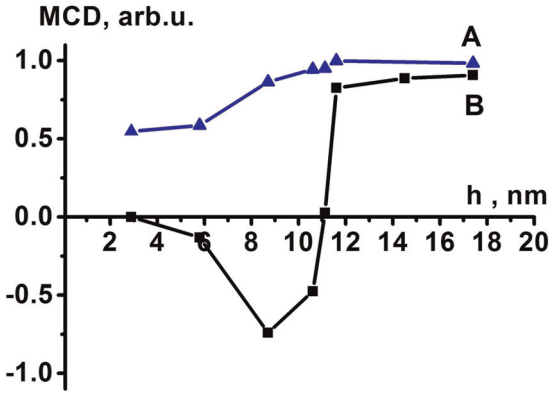

Fig. 5. Thickness dependencies of the long-wave MCD peak signals for the A- and B-type films. (For interpretation of the references to color in this figure legend, the reader is referred to the web version of this article.)

of their composition in the full range of investigated thicknesses, at least when the thickness of the films is above 5.8 nm. The measured Faraday rotation spectra for the A- and B-type films with the thicknesses above 23.2 nm, as well as for the MPCs using such films as magneto-active layers [20,21], are in good agreement with the data reported earlier in [22,23] for the $Bi_3Fe_5O_{12}$ films prepared by reactive beam sputtering. This fact provides an additional confirmation that the film composition is close to nominal for large h. It is worth to be mentioned that for the films prepared by pulsed laser deposition the increase of the thickness from 470 nm to 2560 nm leads to a shift of the maximum position in the MCD spectra from 530 nm to 560 nm [24]. For the rf-magnetron sputtered, $Bi_3Fe_5O_{12}$ films of 1.32 μm and 1.39 μm thickness deposited on (1 1 1) and (0 0 1) GGG substrates the maximum value of FR was observed at $\lambda \approx 550$ nm [25].

The thickness dependencies of the amplitude of the long-wave peak in the MCD spectra for the A- and B-type films are shown in Fig. 5. A positive sign of the peak amplitude is observed for all the A-type film thicknesses. In the B-type films, the amplitude changes its sign from negative to positive with the thickness increase at $h \approx 10.7$ nm, which is in a good agreement with h_{cr} found from the FR measurements (see Fig. 2).

Summarizing the results of the FR and MCD investigations, the following conclusions can be made. According to the MCD measurements, the films with the thickness below 2.9 nm are nonmagnetic at room temperature. In thicker films, this results in formation of a nonmagnetic sublayer on substrate-film interface. The thickness dependencies of the FR and MCD in the B- and C-type films show a formation of transitional layer of about 10–12 nm thick with the variation of the composition due to the intermixture of the materials from the film and substrate (see below). The concentration profile of this transitional layer strongly depends on the substrate pretreatment. One should note that the total thickness of the films was used to calculate θ_F and MCD. If we subtract the thickness of nonmagnetic sublayer, the beginning part of $\theta_F(h)$ and MCD (h) dependencies for the B- and C-type films will be steeper. Using this method, we find that in the A-type films, the variation of θ_F and MCD with thickness is even smaller. So their composition should be close to the target composition even when their thickness is well below 10.6 nm.

To explain the formation of the transitional layer, let us consider the processes taking place onto film-substrate interface during the crystallization annealing of the films. The sign inversion of the FR and MCD signals in the B- and C-type films are possible only if Ga^{3+} and Gd^{3+} ions penetrate into the films from the substrate. This penetration becomes possible due the presence of a damaged amorphous layer on the GGG surface. This layer can even contain

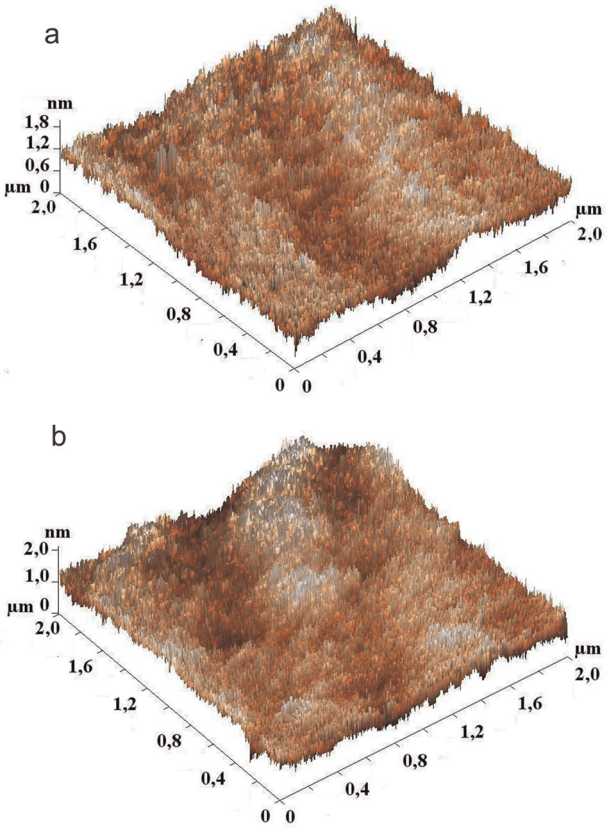

Fig. 6. AFM images of the GGG substrates processed by 1 keV Ar^+ (a) and 4 keV Ar^+ (b) ions. (For interpretation of the references to color in this figure legend, the reader is referred to the web version of this article.)

Ga and Gd oxides. For standard substrates the amorphous layer on surfaces could be formed as a result of their mechanical pretreatment and even a chemical-dynamic polishing cannot totally remove it. However, taking into account the data obtained for the A-type films, the influence of this mechanism is small and can be neglected. A pretreatment of the GGG surface by low-energy Ar^+ (or oxygen) plasma does not lead to a sign change of θ_F and MCD signals. No sign change was observed in the sputtered and in situ crystallized iron-garnet films either [7].

Pre-treatment of GGG substrate surface by Ar^+ ions with high enough energy (1–4 keV), as in the case of the B- and C-type films, leads to an amorphization or possibly a partial destruction of the GGG substrate surface with an appearance of Ga and Gd oxides. In this case, a transitional layer containing the elements of both the film and the substrate is expected to be formed on the interface after film deposition and annealing. With the increasing distance from the substrate, the concentrations of Ga^{3+} and Gd^{3+} ions in the films decrease, while the concentration of Bi^{3+} and Fe^{3+} increase, and thus, a formation of the transitional $(Bi_\alpha Gd_\beta Y_\gamma)_3(Fe_\delta Ga_\varepsilon)_5O_{12}$ layer with a gradual composition variation takes place during the crystallization. The substitution of Fe^{3+} by Ga^{3+} and Bi^{3+} by Gd^{3+} should dramatically affect the magnetic structure and the magneto-optical properties of the films, especially when their thickness is less than or comparable to the thickness of the transitional layer. Strong variations of θ_F and MCD (including their sign change), T_C and T_{comp} with h for the thin B- and C-type films are indeed observed in the experiments. The formation of a similar transitional layers containing a mixture of the elements coming from the substrate and the film, accompanied by the inversion of the Faraday rotation and a variation of the compensation temperature, was studied in [26] for the $(BiSmLu)_3(FeGaAl)_5O_{12}$ thin films grown on GGG by LPE.

The sign inversion of the magneto-optical effects in the B- and C-type films supposes a formation of compensation planes inside the transitional layers [11]. In these planes, the garnet material is antiferromagnetic, and the absolute values of the magnetic moments of the tetrahedral and octahedral sublattices are equal. The magnetic moment compensation is mainly due to Ga^{3+} substitution of Fe^{3+} ions. For example, the compensation takes place in gadolinium iron garnet $Gd_3Fe_5O_{12}$ a little bit below the room temperature $T_{comp} = 286$ K [27] while in gallium substituted iron garnets with Ga^{3+} 1.3 at./f.u. it takes place at room temperature [28]. So it is highly probable that within the compensation planes in the B- and C-type films the composition of the material is $(BiGdY)_3Fe_{3.7}Ga_{1.3}O_{12}$. The position of the compensation plane should coincide with the position of the maximum on θ_F (h) dependencies [29,30] for the B- and C-type films.

The AFM investigations were carried out to determine the morphology of GGG surfaces after different types of ion pretreatment and to characterize the surface morphology of Bi:YIG films deposited on these substrates. The results of the study for B- and C-type substrates and films are shown in Figs. 6–10.

The maximum roughness of the A-and B-type substrates and amorphous films deposited on these substrates does not exceed 1–2 nm and for the C-type substrates and amorphous films is of about 2–3 nm (see Figs. 6 and 7). As for the C-type substrates, it is a rather unexpected result. We supposed much more serious damage on the surface of the substrates bombarded by 4 keV ions. Etching patterns can clearly be seen on the B- and C-type substrates (Fig. 6), but for the C-type substrates, they are even more pronounced. The patterns are typical for low energy ions processing of a surface and usually follow crystallographic directions or the direction of the ion beam [31].

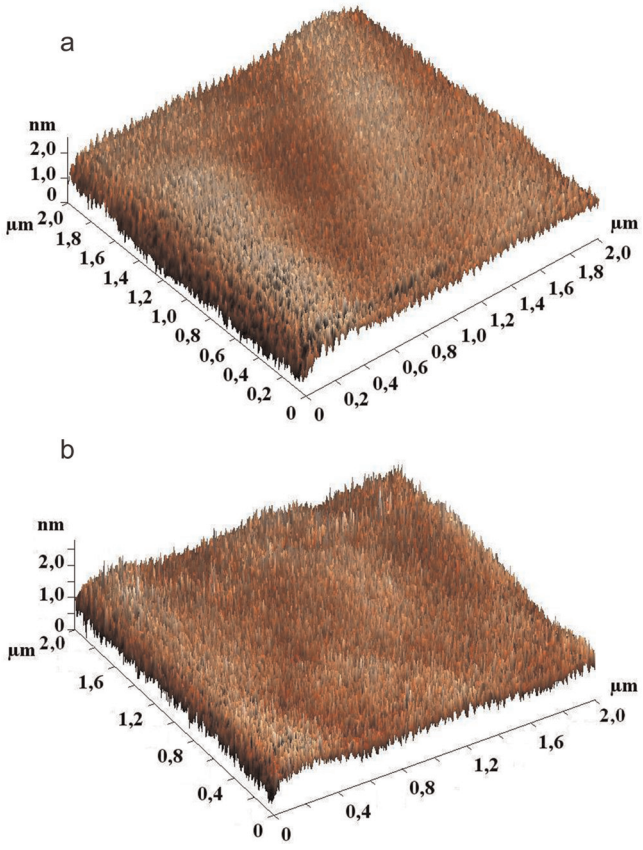

Fig. 7. AFM images of the amorphous B-type (a) and C-type (b) films of 17.4 nm thick. (For interpretation of the references to color in this figure legend, the reader is referred to the web version of this article.)

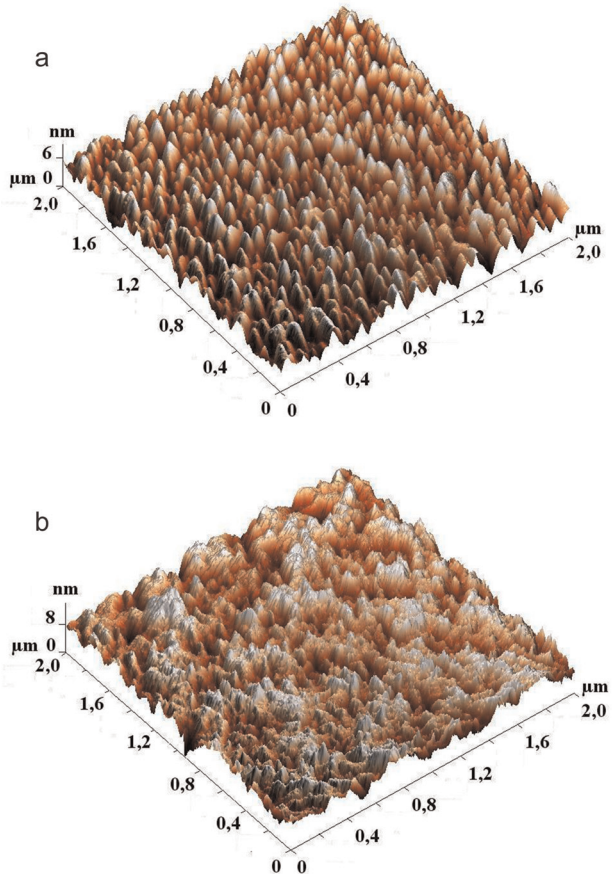

Fig. 8. AFM images of the crystallized B-type (a) and C-type (b) films of 17.4 nm thick. (For interpretation of the references to color in this figure legend, the reader is referred to the web version of this article.)

The crystallization annealing of the deposited films leads to considerable modification of the films surfaces. It should be note that the crystallization processes run differently for the B- and C-type films (see Fig. 8). The crystallites density per unit area in the B-type films is much higher than in the C-type ones, i.e., the crystallites size is significantly smaller. For the B-type films, the maximal height of crystallites is 6 nm, the average height is 4 nm, the average roughness of the surface is 2 nm, and the mean crystallites size is of about 50 nm. In the C-type films, these parameters are 8 nm, 6 nm, 3 nm and 200 nm, respectively.

In the C-type films of 69.6 nm thick, vertexes of crystallites are mainly multi-domed (Fig. 9b) while in the B-type films they are mainly single-domed (Fig. 9a). This difference is also observed for thicker films (Fig. 10). The maximum height of crystallites is 30 nm for the B-type films of 116 nm thickness, their average height is 12 nm, the average roughness is 6 nm, and the mean crystallites size is 220 nm. For the C-type films, these parameters are 57 nm, 30 nm, 13 nm and 400 nm, correspondingly.

The relatively high value of the annealed films roughness is most probably connected with high heating rate during the crystallization. Our preliminary study shows that the annealing with the controlled heating rate of about 2 °C/min leads to 5 times reduction of the crystallites height.

Let us consider the influence of the crystallization annealing on Bi:YIG films formation processes. It is known that monocrystalline defect-free LPE garnet films can be grown on garnet substrates only if there is a lattice mismatch between film and substrate $\Delta a < 0.002$ nm [5]. At these conditions, the formation of {1 1 0} and {2 1 1} crystallographic variants is completely suppressed, and epitaxial films with plane surfaces can be obtained. If $\Delta a \approx 0.006$

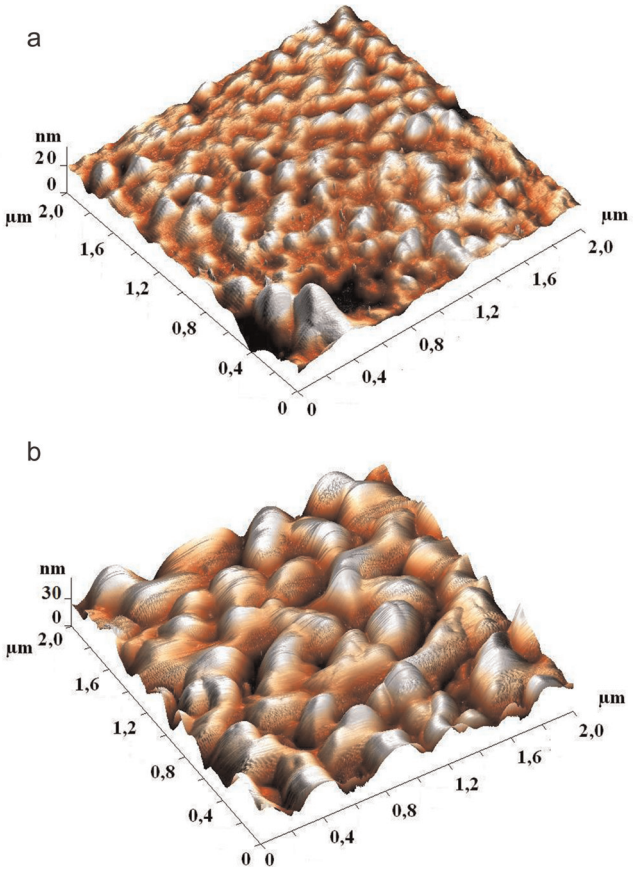

Fig. 9. AFM images of the crystallized B-type (a) and C-type (b) films of 69.6 nm thick. (For interpretation of the references to color in this figure legend, the reader is referred to the web version of this article.)

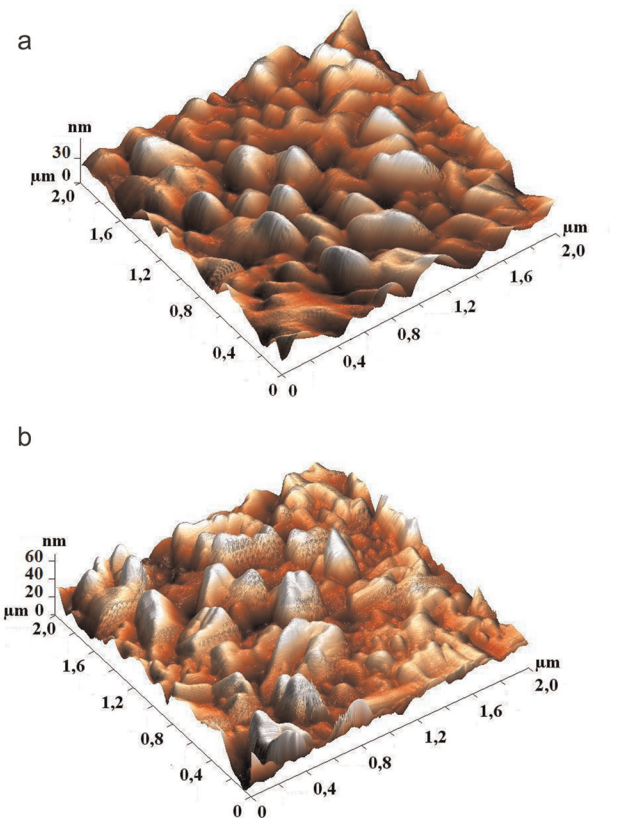

Fig. 10. AFM images of the crystallized B-type (a) and C-type (b) films of 112 nm thick. (For interpretation of the references to color in this figure legend, the reader is referred to the web version of this article.)

nm, oblique columnar structures are usually formed. Meanwhile different sputtering techniques have been successfully used for the preparation of epitaxial Bi:YIG films when $\Delta a > 0.02$ nm [1,5,22,32].

The investigated films have the composition $Bi_{2.8}Y_{0.2}Fe_5O_{12}$, $a_{film} = 1.2602$ nm and $\Delta a = 0.0208$ nm. The growth of such films is possible only when some crystallization centers on GGG substrate surface are present. Such centers can be provided by the defects formed during the substrate surface mechanical polishing. These defects could produce lattice distortions required for epitaxial growth. The centers can be also formed on the substrate surface areas where the lattice parameters change, for instance, as a result of ion-induced effects.

The observed surfaces dissimilarity of the films of different types can be explained in the following assumptions. The main mechanism of nucleation in the A-type films is similar to mechanism of atomically smooth growth. A selective nucleation takes place in the case of the B- and especially of the C-type films. A partial intermixing of the substrate and the film elements should be also taken into account for the B- and C-type films. During the crystallization process in these films, a formation of transitional layer takes place where the lattice parameter, a_{tr}, gradually changes from $a_{sub} = 1.2383$ nm near the substrate to $a_{film} = 1.2602$ nm in thick $Bi_{2.8}Y_{0.2}Fe_5O_{12}$ film. This gradual variation of a_{tr} through the transitional layer thickness also facilitates the epitaxial growth of the films with large Δa.

Indeed, a large number of ion-induced small defects in the B-type substrates should lead to a high density of small crystallites (Fig. 8a). In the C-type films GGG substrate surface has been damaged by high energy Ar^+ ions that leads to formation of large defects, and the film surface is packed with multi-domed crystallites (Fig. 8b). The increase of the films' thickness leads to the growth of the crystallites which are in favorable conditions at the expense of the others. This leads to the increase of the crystallites mean size with the film thickness increase. But the characteristic features of the crystallites remain the same.

In addition, it is worth mentioning that the ultrathin amorphous Bi:YIG films deposited onto cold GGG substrates and crystallized in air at $T_{cryst} = 650\,^{\circ}C$ preserve the information about the original substrate crystalline state, as it is revealed by composition profiles displayed by the sign of magneto-optical effect. This effect in ultrathin Bi:YIG films was named a "memory effect" [33].

4. Conclusion

The sign inversion of the magneto-optical effects was observed in ultrathin $Bi_{2.8}Y_{0.2}Fe_5O_{12}$ films deposited on (111) GGG substrates pretreated by Ar^+ ion beam with the ions energy exceeding 1 keV and annealed in the air. This effect was explained in terms of the substrate surface damage and amorphization as a result of ions bombardment, which leads to partial intermixture of the elements of the film and the substrate and a formation of a transitional $(Bi_\alpha Gd_\beta Y_\gamma)_3(Fe_\delta Ga_\varepsilon)_5O_{12}$ layer with the gradual variation of the composition. The variation of the composition results in the formation of the compensation planes inside the transitional layers and in a change of the compensation point of the films. It has been shown that in ultrathin films the compensation point is above the room temperature. The highest value of specific Faraday rotation $\theta_F = -7.8^{\circ}/\mu m$ at $\lambda = 655$ nm was obtained in 100 nm-thick films deposited on (111) GGG substrates which were annealed in the air and pretreated by oxygen plasma.

Atomic force microscopy was used to study the influence of the substrate surface pre-treatment on the crystallisation of the films. It has been shown that the main mechanism of the growth for the films on the substrates pre-treated by low energy ions is similar to atomically smooth growth, while the high energy ions pre-treatment results in selective nucleation mechanism of the growth.

Controlled ion beam pre-treatment of the substrate opens a pathway to manufacturing thin films with custom-made magneto-optical properties using growth equipment with a single target material for deposition.

Acknowledgments

This work was supported by the State Program of Ukraine "Nanotechnologies and Nanomaterials" grant #1.1.3.27. The authors acknowledge the support from National Academy of Sciences of Ukraine, the Ministry of Education and Science of Ukraine and the State Fund for Fundamental Research and the Faculty of Computing, Health and Science, Edith Cowan University (Australia).

References

[1] T. Okuda, N. Koshizuka, K. Hayashi, H. Taniguchi, K. Satoh, H. Yamamoto, IEEE Translation Journal on Magnetics in Japan 3 (1988) 483–484.
[2] S. Kahl, A.M. Grishin, Applied Physics Letters 84 (2004) 1438–1440.
[3] A.A. Fedyanin, D. Kobayashi, K. Nishimura, H. Uchida, M. Inoue, O.A. Aktsipetrov, Materials Research Society Symposium Proceedings 834 (J1.5) (2005) 1–4.
[4] M. Inoue, H. Uchida, K. Nishimura, P.B. Lim, Journal of Materials Chemistry 16 (2006) 678–684.
[5] A.H. Bobeck, E. Della Torre, Magnetic Bubbles, North Holland Publishing Company, Amsterdam, 1975.
[6] V.A. Kotov, V.I. Burkov, M. Vasiliev, K. Alameh, D.E. Balabanov, V.I. Belotelov, V.G. Shavrov, K.A. Zvezdin, Proceedings of the 5th International Conference ICFM-2009, Crimea, Ukraine, 2009, pp. 199.
[7] J.-P. Krumme, V. Doormann, B. Strocka, P. Willich, Journal of Applied Physics 60 (1986) 2065–2068.
[8] A.I. Stogniy, O. Ochilov, K.M. Mukimov, V.V. Fedotova, G.M. Khalmuratov, H.A. Ramazanov, Zhurnal Tekhnicheskoi Fiziki 66 (1996) 192–197.
[9] A.N. Shaposhnikov, A.R. Prokopov, A.V. Karavainikov, V.N. Berzhansky, I.V. Sharay, V.G. Bar'yakhtar, Proceedings of the 6th International Conference ICFM-2011, Crimea, Ukraine, 2011, pp. 178.
[10] T.V. Mikhailova, V.N. Berzhansky, A.N. Shaposhnikov, A.R. Prokopov, A.V. Karavainikov, V.A. Kotov, L.N. Alyab'eva, V.I. Burkov, D.E. Balabanov, A.S. Baturin, Proceedings of the 6th International Conference ICFM-2011, Crimea, Ukraine, 2011, pp. 186.
[11] V.A. Kotov, V. Shavrov, V. Berzhansky, A. Karavainikov, A. Prokopov, A. Shaposhnikov, D. Balabanov, V. Burkov, Proceedings of the 5th International Congress on Advanced Electromagnetic Materials in Microwaves and Optics, Barcelona, 2011, pp. 66.
[12] A.R. Denton, N.W. Ashcroft, Physical Review A 43 (1991) 3161–3164.
[13] V.N. Berzhansky, A.V. Karavainikov, E.T. Milyukova, T.V. Mikhailova, A.R. Prokopov, A.N. Shaposhnikov, Functional Materials 17 (2010) 120–126.
[14] M. Dep, E. Popova, A. Fouchet, N. Keller, Journal of Physics D: Applied Physics 45 (2012) 455001.
[15] G.F. Dionne, G.A. Allen, Journal of Applied Physics 95 (2004) 7333.
[16] A.K. Zvezdin, V.A. Kotov, Modern Magnetooptics and Magnetooptical Materials, Institute of Physics Publishing, Bristol, 1997.
[17] M.-Y. Chern, F.-Y. Lo, D.-R. Liu, K. Yang, J.-S. Liaw, The Japanese Journal of Applied Physics 38 (1999) 6687–6689.
[18] V. Doormann, J.-P. Krumme, H. Lenz, Journal of Applied Physics 68 (1990) 3544–3553.
[19] F. Hansteen, L.E. Helseth, T.H. Johansen, O. Hunderi, A. Kirilyuk, T. Rasing, Thin Solid Films 455–456 (2004) 429–432.
[20] V.N. Berzhansky, A.N. Shaposhnikov, A.R. Prokopov, A.V. Karavainikov, T.V. Mikhailova, E.Y. Semuk, M.I. Sharipova, T.V. Dolgova, A.A. Fedyanin, V.A. Kotov, V.O. Golub, Materialwissenschaft und Werkstofftechnik 42 (2011) 19–23.
[21] V.N. Berzhansky, T.V. Mikhailova, A.V. Karavainikov, A.R. Prokopov, A.N. Shaposhnikov, I.N. Lukienko, Yu.N. Kharchenko, O.V. Miloslavskaya, N.F. Kharchenko, Journal of the Magnetics Society of Japan 36 (2012) 42–45.
[22] T. Ocuda, N. Koshizuka, K. Hayashi, K. Satoh, H. Tanigushi, H. Yamamoto, Proceedings of the 12th Internatuinal Colloquium on Magnetic Films and Surfaces, Le Creuson, France, 1988, pp. 204–205.
[23] T. Ocuda, T. Katayama, K. Satoh, T. Oicawa, H. Yamamoto, N. Koshizuka, Proceedings of the 5th Symposium on Magnetism and Magnetic Materials "Recent Advantages in Magnetism and Magnetic Materials", Taipei, Taiwan, 1989, pp. 61–76.
[24] S. Kahl, A.M. Grishin, Journal of Magnetism and Magnetic Materials 278 (2004) 244–255.
[25] P. Johansson, S.I. Khartsev, A.M. Grishin, Thin Solid Films 515 (2006) 477–480.
[26] V.N. Berzhansky, A.V. Karavainikov, E.T. Milyukova, A.R. Prokopov, A.N. Shaposhnikov, Functional Materials. 17 (2010) 177–183.
[27] M.A. Gilleo, in: E.P. Wohlfarth (Ed.), Ferromagnetic Insulators: Garnets Handbook of Magnetic Materials, 2, North-Holland Publishing Company, Amsterdam, 1980.
[28] I. Syvorotka, Electrical Engeneering 60 (2009) 168–175.
[29] J.-P. Krumme, P. Hansen, Applied Physics Letters 22 (1973) 312–314.
[30] L. Wilkens, D. Trager, H. Dotsch, A.M. Alexeev, A.F. Popkov, V.I. Komlev, Journal of Applied Physics 93 (2003) 2839–2847.
[31] W.L. Chan, E. Chason, Journal of Applied Physics 101 (2007) 121301-1–121301-46.
[32] S. Leitenmeier, T. Koerner, J. Griesbauer, M. Herbort, Journal of Crystal Growth 310 (2008) 5392–5401.
[33] A.R. Prokopov, A.N. Shaposhnikov, A.V. Karavainikov, V.A. Kotov, V.N. Berzhansky, Proceedings of the Moscow International Symposium on Magnetizm (MISM 2011), Moscow, Russia, 2011, pp. 212.